ECHOCARDIOGRAPHIC SIMULATION FOR VALIDATION OF AUTOMATED SEGMENTATION METHODS

Andrew D. Gilliam and Scott T. Acton

C. L. Brown Dept. of Electrical & Computer Engineering
University of Virginia, Charlottesville, Virginia, USA
[drew.gilliam, acton]@virginia.edu

ABSTRACT

Segmentation of echocardiographic imagery is central to the understanding, diagnosis, and treatment of cardiovascular disease. Although volumes of literature have been devoted to automated image segmentation, little work has been directed towards the validation of these techniques. An echocardiographic simulation has the advantage of exact knowledge of the myocardial borders, thus providing quantifiable measurements of an algorithms performance. Existing simulation tools either become intractable when generating multiple images, or accommodate only simplistic myocardial motion models. This paper proposes a novel tool for the simulation of short-axis echocardiographic image sequences towards the goal of automated segmentation algorithm validation. We consider a complete set of simulation concerns, including a realistic myocardial model, variable inter-frame speckle pattern correlation, and low computational cost for fast simulation. We demonstrate the value of the proposed tool by evaluating a speckle filtering algorithms effects on segmentation accuracy.

Index Terms: Image analysis, image segmentation, image simulation, ultrasound.

1. INTRODUCTION

Segmentation of echocardiographic imagery provides researchers and clinicians with quantifiable measurements of vital physiological parameters. For example, segmentation results may be employed in the calculation of cardiac output or local myocardial strain. These measurements are central to the understanding, diagnosis, and treatment of cardiovascular disease. Traditionally, the myocardium is manually delineated by a trained technician in a tedious, time consuming, and highly variable process. Automated segmentation algorithms provide a fast and accurate alternative.

Robust validation of automated echocardiographic segmentation is largely ignored in the image processing community. Researchers often base algorithm performance solely on statistical comparisons with manual segmentation results which suffer from inter- and intra-observer error. An echocardiographic simulation, however, has the advantage of a priori knowledge of the exact myocardial border location and can provide compelling quantifiable measurements of an algorithms accuracy and precision.

A pervasive ultrasound simulation tool, FIELD II, has the ability to simulate B-mode ultrasound imagery [1, 2]. However, FIELD II becomes intractable when attempting to simulate multiple images, and does not include the ability to simulate correlated multi-frame sequences. Other researchers have previously made efforts to develop an echocardiographic simulation [3-5]. These simulations, however, consider simplistic myocardial motion models which ignore important parameters such as cardiac twist.

In this paper, we propose a novel tool for the simulation of short-axis echocardiographic image sequences. We consider a complete set of simulation concerns, including a realistic myocardial model, variable inter-frame speckle pattern correlation, and low computational cost for fast simulation. The next two sections discuss the myocardial model and ultrasound simulation method, respectively. We conclude with a discussion of the simulation including execution speed, an example algorithmic validation, and future research directions.

2. MYOCARDIAL MODEL

Figure 1 illustrates a typical short axis echocardiographic image. To create an analogous simulation, we must first define the myocardial borders at end-diastole and end-systole. We then define our motion model, and finally determine movement throughout the full region of interest.

2.1. Myocardial border definition

The myocardium is first defined according to two unique borders at two unique time points in the cardiac cycle, i.e. the outer (epicardial) and inner (endocardial) borders at both end-diastole and end-systole. Each border is modeled as an

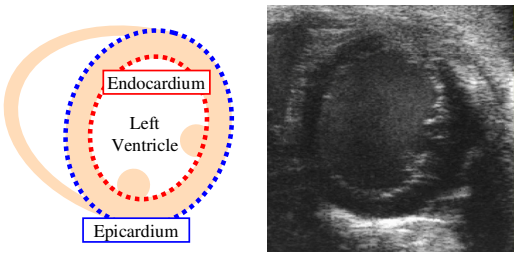

Figure 1. B-mode short-axis myocardial diagram and typical echocardiographic image.

ellipse [6], parameterized by the ellipse center, major-axis diameter, minor-axis diameter, and orientation.

2.2. Myocardial motion model

We simulate myocardial motion via an affine transformation between the end-diastolic and end-systolic contours, allowing for myocardial contraction as well as an underlying rigid body motion.

Let $[x_D,y_D]$ and $[x_S,y_S]$ represent the endocardial (or epicardial) contour at end-diastole and end-systole, respectively. The relationship between these two contours can be defined as an affine transformation

$$A = \begin{bmatrix} \rho_x \cos\theta & -\rho_y \sin\theta & \delta_x \\ \rho_x \sin\theta & \rho_y \cos\theta & \delta_y \\ 0 & 0 & 1 \end{bmatrix}, \qquad \begin{bmatrix} x_S & y_S & 1 \end{bmatrix}^T = A \cdot \begin{bmatrix} x_D & y_D & 1 \end{bmatrix}^T \tag{1}$$

consisting of lateral and axial translations δ_x and δ_y, lateral and axial scaling ρ_x and ρ_y, and rotation θ. These affine parameters are easily determined from the ellipse parameters mentioned in Section 2.1.

To determine the contour $[x(t),y(t)]$ at an arbitrary time point t within the cardiac cycle, we apply a weighting function $w(t) \in [0,1]$ to the affine parameters as follows:

$$\begin{aligned} \gamma(t) &= w(t) \cdot \delta \\ \alpha(t) &= 1 - w(t) \cdot (1-\rho) \\ \beta(t) &= w(t) \cdot \theta \end{aligned} \tag{2}$$

This produces the corresponding affine matrix $B(t)$

$$B(t) = \begin{bmatrix} \alpha_x(t)\cos\psi(t) & -\alpha_y(t)\sin\psi(t) & \gamma_x(t) \\ \alpha_x(t)\sin\psi(t) & \alpha_y(t)\cos\psi(t) & \gamma_y(t) \\ 0 & 0 & 1 \end{bmatrix}, \qquad \begin{bmatrix} x(t) & y(t) & 1 \end{bmatrix}^T = B(t) \cdot \begin{bmatrix} x_D & y_D & 1 \end{bmatrix}^T \tag{3}$$

The weighting function $w(t)$ may be any smoothly varying continuous function, varying between zero and one. When $w(t)$=0, $B(t)$ is the identity matrix and we thus produce the end-diastolic contour. When $w(t)$=1, $B(t)$ is A and we thus produce the end-systolic contour. Figure 2 illustrates a typical weighting function, derived from a standard left ventricular volume diagram [6].

In addition to the contractile and rigid body motion modeled via the affine transformation, we have included an additional parameter to model cardiac twist [7]. The twist angle allows points to move along the contour, independent of the underlying ellipse change, as illustrated in Figure 3.

2.3. Motion field

Given myocardial motion throughout the cardiac cycle, we are able to define motion in arbitrary space utilizing the piecewise linear transformation technique described in [8]. We simulate a moving object within an elastic medium, where the medium is fixed along the image border.

Let $[u_0,v_0]$ represent the end-diastolic point set, consisting of discrete points along the end-diastolic contours and fixed points along the image borders. Let $[u(t),v(t)]$ represent the point set at an arbitrary time t within the cardiac cycle, consisting of discrete points along the myocardial contours and the same fixed points along the image borders. Note that points in $[u_0,v_0]$ and $[u(t),v(t)]$ have a one-to-one correspondence.

We tessellate the end-diastolic image field into smaller regions via a Delaunay triangulation of $[u_0,v_0]$ [9]. Figure 4 illustrates a typical end-diastolic Delaunay triangulation, along with several corresponding triangles in an arbitrary frame. We then infer an affine mapping from $[u_0,v_0]$ to $[u(t),v(t)]$ for each triangle. Arbitrary points within the image field move according to the motion of the surrounding triangle. Thus, we define movement throughout the region of interest, driven by our myocardial contours. A typical motion field is illustrated in Figure 5.

3. ULTRASOUND SIMULATION

With a well defined myocardial model and the corresponding motion field, we are able to define the ultrasound simulation model. We define a scatterer field, aquire an image of the field with our simulated imaging system, and reconstruct the resulting radio frequency (RF)

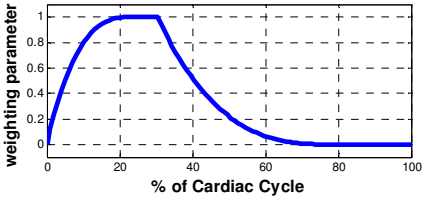

Figure 2. Example weighting function.

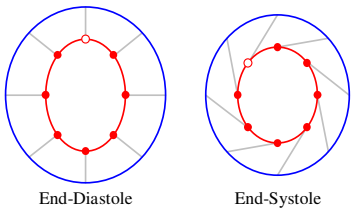

Figure 3. Endocardial twist illustration.

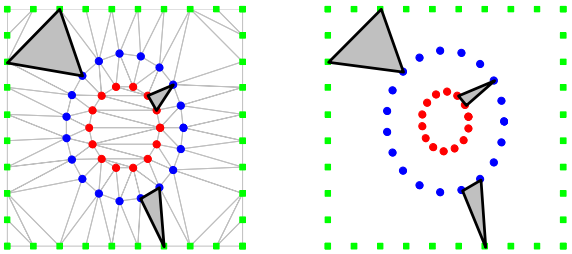

Figure 4. Delaunay triangulation and correspondence.

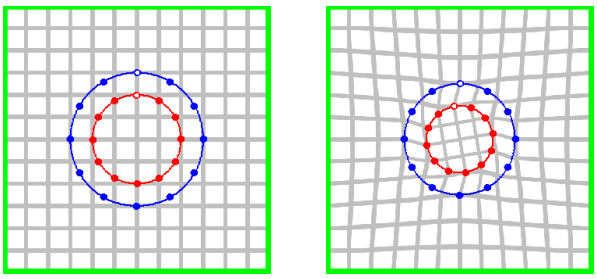

Figure 5. Piecewise linear spatial transformation.

data into a recognizable echocardiographic sequence. Our simulation is based on the image formation models presented in [10] and [11].

3.1. Scatterer field

Homogeneous tissue is generally modeled as a collection of point scatterers with Gaussian distributed scattering amplitudes. To reduce computational complexity, we arrange point targets into a 2D matrix with uniform lateral spacing and uniform axial spacing. Axial spacing must satisfy the Nyquist criterion, i.e. point target frequency in the axial direction must be greater than twice the imaging system spatial frequency.

We generate an end-diastolic scatterer matrix via a variance map, which defines the scatterer amplitude variance in different spatial regions. Figure 6 illustrates a typical end-diastolic myocardial definition and the corresponding variance map. The increased variance at horizontal borders simulates a transducer positioned at the top of the image receiving strong reflections from interfaces perpendicular to the sound wave direction of travel.

To obtain a correlated scatterer sequence, we warp the end-diastolic scatterer matrix according to the piecewise linear motion field described in Section 2.3. The blood pool, however, is randomized at each time instance as blood is uncorrelated from frame to frame (a unique feature of our model that parallels the real imaging scenario).

3.2. Image acquisition

An echocardiographic linear imaging array typically acquires multiple radio frequency (RF) axial lines across the lateral dimension of the tissue. The RF signal at any point $[x,y]$ can be modeled as a 2D spatial convolution of the

Figure 6. End-diastolic myocardium and variance map.

tissue impulse response $A(x,y)$ with the imaging system point spread function (PSF) $h(x,y)$, i.e.

$$RF(x,y) = \int_{\Re^2} A(u,v) \cdot h(x-u, y-v)\, du\, dv \cdot \qquad (4)$$

Taking the tissue impulse response as the aforementioned scatterer matrix, our RF signal is thus a simple spatial convolution with manageable computational complexity.

The imaging system PSF can be modeled by a number of functions, determined theoretically or experimentally. We define a spatially-invariant PSF of the form

$$h(x,y) = \frac{1}{2\pi\sigma_x\sigma_y}\exp\left(-\frac{x^2}{2\sigma_x^2}-\frac{y^2}{2\sigma_y^2}\right)\cdot\sin\left(2\pi\tfrac{f_0}{c}y\right), \qquad (5)$$

where σ_x and σ_y are the lateral and axial PSF dimensions, c is the assumed speed of sound, f_0 is the system frequency (Hz), and f_0/c is the system spatial frequency (1/m).

To better replicate a typical system output, after convolution we choose N axial lines from our RF data set. Thus, we obtain N RF axial lines sampled at the system sampling frequency, separated by some lateral spacing, prior to the reconstruction step.

3.3. Image reconstruction

To obtain the image as seen by a echocardiographic technician, we apply some simple image reconstruction and post-processing techniques to the RF data. We first detect the baseband signal from the RF data via a Hilbert transform. We then interpolate the baseband data set over some uniformly sampled output space. Finally, we log-compress the resultant image and saturate at some decibel level. Figure 7 shows a four frame image sequence after reconstruction ranging from end-diastole to end-systole.

4. RESULTS & DISCUSSION

This paper proposed a novel tool for the simulation of short-axis echocardiographic image sequences towards the goal of validating/comparing segmentation performance. We extended the efforts of existing tools by addressing a more complete set of simulation concerns, including a realistic myocardial model, variable inter-frame speckle pattern correlation, and greatly reduced execution times. This simulation tool will advance the state-of-the-art in the

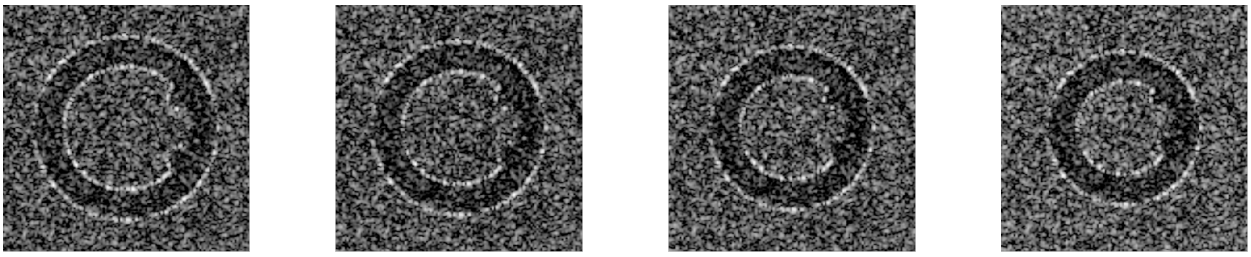

Figure 7. (left) End-diastolic to (right) end-systolic simulated echocardiographic image sequence.

comparison and evaluation of echocardiographic image sequence segmentation.

For comparison, we simulated a single FIELD II image of 100,000 scatterers with 128 A-lines on a 3.6GHz Pentium 4 processor with 2GB RAM. This single image took over 6 hours to create, which would result in a 15 frame execution time of at least 3.75 days. Our simulation method, on the same system with comparable parameters, had an execution time of 140 seconds for a full 15 frame sequence. This is an over 2000 times execution time reduction .

To demonstrate the value of the proposed simulation as a validation tool, we attempted to quantify the effectiveness of speckle reducing anisotropic diffusion (SRAD) [12] as a pre-processing tool for echocardiographic segmentation. SRAD attempts to smooth homogenous tissue regions while preserving feature edges, thus improving segmentation accuracy.

We simulated five sequences, each containing ten frames, and attempted segmentation both before and after SRAD filtering. Each frame was segmented independently using an active contour approach [13] with a generalized gradient vector flow [14] external force. All contours were identically initialized and run until convergence. On average, SRAD filtering prior to segmentation provided 34% and 54% reductions in endocardial and epicardial RMSE, respectively. Figure 8 illustrates segmentation results before and after SRAD.

The proposed simulation tool can be advanced in a number of ways. Increasingly accurate myocardial models, or even use of experimental data, can supplement the existing model. Various other echocardiographic characteristics are being considered, including shadowing, rib artifacts, a spatially variant PSF, and more faithful ultrasound reconstruction methods. Additionally, other echocardiographic imaging modes, such as long-axis myocardial imagery, could benefit from a similar tool.

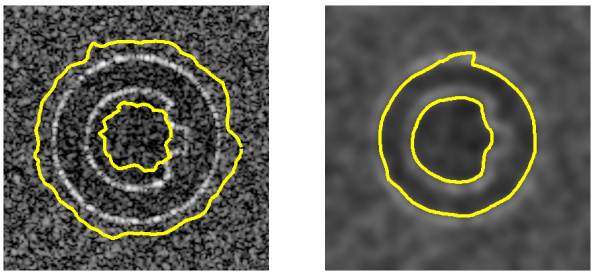

Figure 8. Segmentation (left) before and (right) after SRAD.

Our cardiac simulation software will be available (by the time of ICIP'07) for download at viva.ee.virginia.edu.

REFERENCES

[1] J. A. Jensen, "Field: A Program for Simulating Ultrasound Systems," Medical & Biological Engineering & Computing, 10th Nordic-Baltic Conference on Biomedical Imaging, vol. 34, supplement 1, part 1, pp. 351-353, 1996b.

[2] J. A. Jensen and S. Nikolov, "Fast simulation of ultrasound images," in IEEE Ultrasonics Symposium. Puerto Rico, 2000.

[3] V. Grau and J. A. Noble, "Motion-guided anisotropic filtering of ultrasound sequences," in IEEE International Symposium on Biomedical Imaging, 2006, pp. 209.

[4] M. J. Ledesma-Carbayo, J. Kybic, M. Desco, A. Santos, M. Suhling, P. Hunziker, and M. Unser, "Spatio-temporal nonrigid registration for ultrasound cardiac motion estimation," Medical Imaging, IEEE Transactions on, vol. 24, pp. 1113, 2005.

[5] M. Suhling, M. Arigovindan, C. Jansen, P. Hunziker, and M. Unser, "Myocardial motion analysis from B-mode echocardiograms," Image Processing, IEEE Transactions on, vol. 14, pp. 525, 2005.

[6] A. D. McCulloch, "Cardiac Biomechanics," in The Biomdeical Engineering Handbook, J. D. Bronzino, Ed., 2nd ed. Boca Ration: CRC Press, LLC, 2000, pp. 28.1-28.26.

[7] W. D. Gilson, Z. Yang, B. A. French, and F. H. Epstein, "Measurement of myocardial mechanics in mice before and after infarction using multislice displacement-encoded MRI with 3D motion encoding," Am J Physiol Heart Circ Physiol, vol. 288, pp. H1491-1497, 2005.

[8] A. Goshtasby, "Piecewise linear mapping functions for image registration," Pattern Recognition, vol. 19, pp. 459-466, 1986.

[9] C. B. Barber, D. P. Dobkin, and H. T. Huhdanpaa, "The Quickhull Algorithm for Convex Hulls," ACM Transactions on Mathematical Software, vol. 22, pp. 469-483, 1996.

[10] J. C. Bamber and R. J. Dickinson, "Ultrasonic B-scanning: a computer simulation," Physics in Medicine and Biology, vol. 25, pp. 463, 1980.

[11] J. Meunier and M. Bertrand, "Ultrasonic texture motion analysis: theory and simulation," Medical Imaging, IEEE Transactions on, vol. 14, pp. 293, 1995.

[12] Y. Yongjian and S. T. Acton, "Speckle reducing anisotropic diffusion," Image Processing, IEEE Transactions on, vol. 11, pp. 1260, 2002.

[13] M. Kass, A. Witkin, and D. Terzopoulos, "Snakes: Active Contour Models," International Journal of Computer Vision, vol. 1, pp. 321-331, 1988.

[14] C. Xu and J. L. Prince, "Generalized gradient vector flow external forces for active contours," Signal Processing, vol. 71, pp. 131-139, 1998.